Evolution of photonic structure on deformation of cholesteric elastomers

P. Cicuta, A. R. Tajbakhsh, and E. M. Terentjev
Cavendish Laboratory, University of Cambridge, Madingley Road, Cambridge CB3 0HE, United Kingdom
(Received 19 October 2001; published 29 April 2002)

We subject a monodomain cholesteric liquid crystal elastomer to uniaxial strain perpendicular to its helical axis and study the response of its texture to deformation. A combination of mechanical, optical, and x-ray scattering measurements confirms the prediction for the director rotation, coarsening, and then unwinding the cholesteric helix. The study of optical absorption of circularly polarized light quantifies the complex dependence of the photonic band-gap structure on strain and directly relates to the microscopic deformation of elastomer. Agreement is found with the recently proposed theoretical prediction of the photonic structure of cholesteric elastomers.

DOI: 10.1103/PhysRevE.65.051704 PACS number(s): 61.41.+e, 42.70.Qs, 83.80.Xz

I. INTRODUCTION

Liquid crystal elastomers are materials displaying both a broken orientational symmetry and a sparsely cross-linked rubbery network of flexible polymers. They have complex mechanical behavior arising from the coupling of the orientational degrees of freedom of the liquid crystalline order and those of the rubber-elastic matrix. In particular, soft deformations and unusual thermal and photoactuation have been discovered and studied in the aligned monodomain nematic phase of rubbers [1–3].

Cholesteric liquid crystals have attracted much interest over the years due to their exciting optical properties [4]. Cholesterics have also found use in very diverse products ranging from thermometers to fabric dyes. There has been an effort for some time to produce and study well-aligned cholesteric liquid crystal polymers and their cross-linked networks–permanently stabilized cholesteric liquid crystal elastomers (CLCE). Much success has been achieved in developing cholesteric polymers [5–7], aligning them by electric and magnetic fields and by surface interactions with substrates. However, the permanent chemical cross-linking of cholesteric textures and obtaining freely standing, mechanically stable rubbery films of such polymers has proven to be much more difficult. Early experiments achieved cholesteric order through the mechanical deformation of an elastomer doped with a low mass chiral liquid crystal [8]. A second approach has been to form a perfect cholesteric texture between parallel cell surfaces and then forming a cross-linked network by UV polymerization [9,10]. While these approaches led to materials with interesting properties and enabled, for example, the study of piezoelectric effects [8,10], they are not ideal. In the first method, the alignment is only induced mechanically and it is not a permanent property of the material, while in the second method only very thin films elastomers can be synthesized and they cannot be used as freely standing samples. Recently a new method of synthesis was devised that solves both problems. Free standing strips of single-crystal, well-aligned cholesteric rubber have been produced by Kim and Finkelmann [11] and a uniform orientation of helical director texture has been confirmed by selective reflection measurements. The key idea of this new method is the use of anisotropic (uniaxial) deswelling induced in a laterally constrained film of a weakly cross-linked cholesteric polymer; the resulting effective biaxial planar extension leads to macroscopic orientation of the director in the plane and, therefore, the helical axis perpendicular to the sample plane. This orientation is then locked by a second-stage cross linking of the network.

In a cholesteric liquid crystal the periodicity of helical structure (characterized by the pitch p and the wave number $q_0=\pi/p$), combined with the local birefringence of the liquid crystal (Δn), forbids propagation of circularly polarized light with the corresponding handedness and the wavelength $\Lambda_{gap}=p\,\Delta n$, determining a photonic band gap. This has been first observed in an elastomer in Refs. [9,11] as the selective reflection of light. The remarkable property of cholesteric elastomers is that Λ_{gap} is tunable, responding to mechanical deformation, as it has been theoretically predicted in Ref. [12] and experimentally observed in Ref. [13]. These materials have many potential applications as novel optical filters and mirrors. It has been demonstrated how a dye-doped CLCE can form the basis of a mirrorless laser whose wavelength can be controlled through mechanical deformation [13].

Theoretical work, describing CLCE and their response to mechanical deformation, predicted a number of new effects, including a very rich and complex evolution of photonic band structure [14,15]. Briefly, when a rubber with cholesteric liquid crystalline microstructure is stretched uniaxially in the x direction, perpendicular to the helix axis z, as in Fig. 1, two main phenomena are expected to occur. First, there is a contraction in the z direction, due to the rubber incompressibility, whose detail depends on the complex transverse anisotropy of the cholesteric helix. Second, the uniform helical rotation of the optical axis (the local nematic director) is disrupted and the helix coarsens, thus producing complex nonlinear corrections to the resulting optical response.

In this paper we study experimentally the effect of uniaxial strain on a CLCE. In marked contrast to the previously studied biaxial strain [13], a uniaxial deformation does not simply reduce the helical pitch but produces a complex photonic structure that modifies with deformation. We present optical absorption and x-ray diffraction measurements on a CLCE sample as a function of strain and discuss

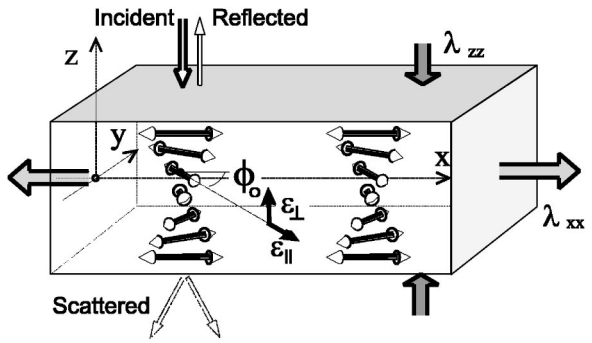

FIG. 1. Diagram of the CLCE geometry showing the cholesteric helical texture characterized by the uniform director rotation about the pitch axis *z*. In our experiments the uniaxial strain $\lambda = \lambda_{xx}$ is imposed along *x*; the associated contraction of sample thickness is λ_{zz}. The incident light and x-ray beams are sent parallel to the pitch axis, resulting in the selective reflection and transmission for light and scattering for x rays.

the complex behavior that is induced even by small uniaxial deformations.

II. METHODS

A. Materials and preparation

A new CLCE was synthesized following the general method introduced by Kim and Finkelmann [11]. Siloxane backbone chains were reacted under centrifugation at 7000 rpm with 90 mol % mesogenic side groups [the nematic 4-pentylphenyl-4′-(4-buteneoxy)benzoate, labeled PBB, and Cholesterol Pentenoate ChP in proportion 4:1] and 10 mol % of 1,4 di(11-undeceneoxy)benzene, di-11UB, cross-linker groups for 45 min at 75 °C to form a partially cross-linked gel. For the further 4 h the reaction proceeded under centrifugation at 60 °C, during which time the solvent was allowed to evaporate, leading to an anisotropic deswelling of the gel and completion of cross linking. All of the volume change in this setup occurs by reducing the thickness of the gel, while keeping the lateral dimensions fixed (due to centrifugation): this introduces a very strong effective biaxial extension in the plane. At this second-stage temperature of 60 °C the dried polymer is in the cholesteric phase and its director is forced to remain in the plane of stretching—this results in the uniform cholesteric texture. The structure of the material produced is shown in Fig. 2. This kind of synthesis produces a very homogeneous strip of elastomer whose size is of the order of 20 cm × 1 cm × 200 μm. Differential scanning calorimetry (DSC) measurements (Perkin-Elmer Pyris 7 DSC) were used to characterize the resulting elastomer. The glass transition was unambiguously determined at $T_g \approx -10$ °C and the clearing point, the isotropic-cholesteric transition occurs at $T_c \approx 90$ °C. No additional thermal transitions were found between these two critical temperatures. All experiments were performed at room temperature, sufficiently far from both transitions.

B. Mechanical measurements

The stress-strain measurements were performed on a custom built device consisting of a temperature compensated

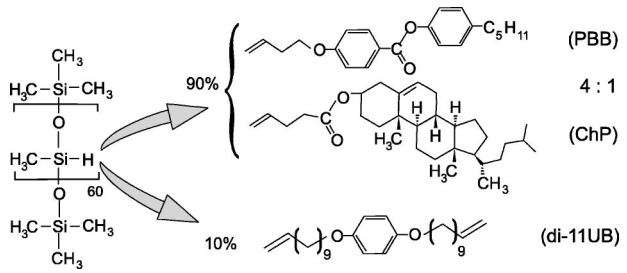

FIG. 2. Chemical structures of the compounds forming the cholesteric elastomer under investigation. A siloxane backbone chain reacting with 90 mol % mesogenic side groups and 10 mol % of the flexible difunctional cross-linking groups (di-11UB). The rodlike mesogenic groups are divided in the proportion 4:1 between the nematic 4-pentylphenyl-4′-(4-buteneoxy)benzoate (PBB) and the derivative of chiral cholesterol pentenoate (ChP).

stress gauge and controller (UF1 and AD20, from Pioden Controls Ltd.) in a thermostatically controlled chamber (Cal3200 from Cal Controls Ltd.). The long elastomer strips were mounted with clamps and extended with a micrometer. The resulting force (as well as the current temperature) values were acquired by connection to a Keithley multimeter (2000 series) and stored on a PC over an IEEE interface. Data obtained in arbitrary units were converted to nominal stress in units of $\mathrm{mN/mm^2} = 10^3$ Pa by calibration with weights.

C. X-ray scattering

Wide-angle x-ray scattering measurements were performed at room temperature with monochromatic Cu$K\alpha$ radiation of 0.154 nm, using a two-dimensional photographic plate. Images were then digitalized and analyzed to extract the azimuthal distribution of intensity indicating the degree of uniaxial order. As with the optical measurements, the beam was incident in the cholesteric pitch direction *z*, and measurements were performed as a function of applied uniaxial strain λ_{xx}.

D. Visible light absorbance

Absorption measurements in the direction of the cholesteric pitch (Fig. 1) were made at room temperature with an HP-8453 UV/visible spectrophotometer, modified so that incident light reached the sample after being transmitted through a linear polarizer and a Fresnel rhomb. Since the Fresnel rhomb is an achromatic quarter-wave retarder, this arrangement produces circularly polarized light throughout the visible spectrum [16] with minimal losses of intensity. The handedness of circular polarization is determined by the orientation of the linear polarizer. An instrumental cutoff, due to both the polarizer and the glass prism, is apparent at ~ 320 nm (Fig. 3). We have measured the transmitted light, and hence will present the data as the ratio I/I_0 of transmitted to incident light. It is a property of the cholesteric materials under study that the fraction of light that is not transmitted is not absorbed by the sample, but mostly reflected backwards. We comment that the direct measurement of the reflected beam would reduce any effects of scattering from

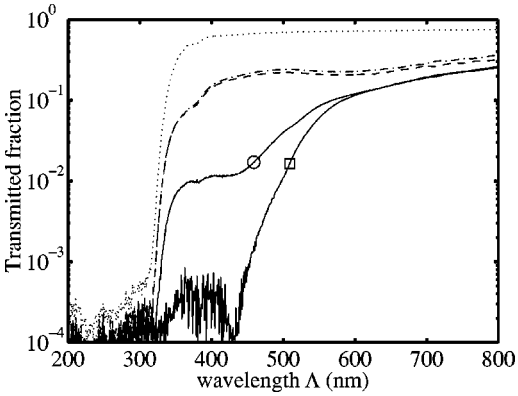

FIG. 3. The absorption due to the Fresnel rhomb (dots) and the baseline absorption due to the complete circular polarizer assembly for L^* (dashed line) and R^* (dash-dot line) polarizations. The fraction of transmitted light (I/I_0, logarithmic scale) for the equilibrium unstretched monodomain CLCE is shown by solid lines, labeled by the circle for L^* and by the square for R^* circular polarizations.

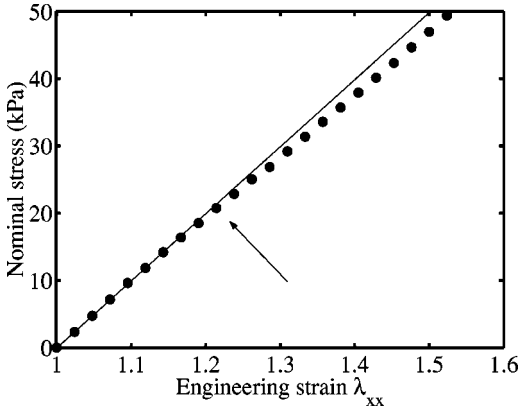

FIG. 4. Stress-strain response of monodomain CLCE stretched uniaxially in the direction perpendicular to the helix. The value of linear rubber modulus at small deformations is $\mu \approx 89$ kPa. The arrow indicates the breaking point of the initial linear regime; its strain $\lambda^* \sim 1.25$.

the sample, but would not extend the accessible range to the UV where the elastomer is not transparent.

III. RESULTS

The first, most intuitively obvious effect occurring on uniaxial stretching of a monodomain cholesteric elastomer across its helical axis is the gradual unwinding of the director helix. As the theoretical model [12] predicted for liquid crystalline polymers with prolate anisotropy of the backbone (chain preferentially extended along the local director), on application of uniaxial strain the director tends to align along the stress axis. This is resisted by the anchoring of the local director in the bulk of the material to the initial helical texture frozen-in by the network cross links. We first examine the mechanical response of such a system and analyze the director distribution from the x-ray scattering data. Having qualitatively confirmed the theoretical prediction of the helix coarsening and eventual unwinding via a continuous set of highly nonuniform director textures, we then study how these affect the photonic band structure of the material.

A. Stress-strain response

The equilibrium stress-strain curve of cholesteric rubber stretched perpendicular to its helix axis could be expected to possess anomalies, since the complex pattern of internal director rotation should follow the deformation; this often is a requirement for soft-elastic response. However, the detailed theoretical calculation [14] has shown that in this geometry (cf. Fig. 1) the rotations are not soft. In fact, only a small anomaly is predicted (within this ideal molecular model) at the critical point of transition where the coarsened winding texture transforms into the nonhelical coarsened wagging regime. The estimate of critical strain for this discontinuous transition, $\lambda_c = r^{2/7}$, is related to the effective parameter of backbone anisotropy r. This is the single parameter of the ideal theory of nematic (and cholesteric) elastomers; $r = \ell_\parallel / \ell_\perp$ is interpreted as the average ratio of backbone chain step lengths along and perpendicular to the local director. r could be directly measured by examining the uniaxial thermal expansion of nematic rubber. Recently much attention has been paid in evaluating this parameter [17,18] and directly relating it to the local value of underlying nematic order parameter $Q(T)$. To a good approximation a relationship $r \approx (1+\alpha Q)^3$ holds with a coefficient α taking a value $\alpha \sim 0.9-1$ for the side-chain siloxane liquid crystalline elastomer cross linked by the flexible linkages, as shown in Fig. 2.

Figure 4 shows the experimentally measured stress-strain curve for our CLCE. The mechanical response is essentially linear for strains up to 20–25 %. In this regime the linear rubber modulus is $\mu \approx 89$ kPa, consistent with other measurements performed on nematic materials with similar composition and cross-linking density. There is a break in the linear stress-strain relation, emphasized by the arrow in the plot. We could attribute this to the theoretically predicted anomaly [14], when at a critical strain λ_c the stress drops below the linear regime. If so, then the value of local backbone anisotropy $r = \lambda_c^{7/2} \approx 2.2$, which is not far from the typical values measured in similar nematic rubbers (r between 2.5 and 3 are reported for such materials). The little discrepancy in the values of r is to be expected: the usual monodomain nematic rubbers are prepared by two-step cross linking with the uniaxial strain of up to 300%, while the cholesteric monodomain was prepared under the effective biaxial strain of much lower magnitude–hence, perhaps, the slightly lower value of effectively frozen chain anisotropy.

B. Helix coarsening and unwinding

Figure 5 shows x-ray scattering patterns for the equilibrium (unstretched) cholesteric rubber (a) and the same rubber stretched by $\lambda_{xx} = 1.4$ (b). In this scattering geometry, the wide-angle diffraction is due to the characteriztic dimension given by the thickness of the aligned and densely packed mesogenic rods [19], averaged over the local director rotating along the z axis. The scattered intensity around this ring is initially uniform, see Fig. 5(a), indicating that the nematic

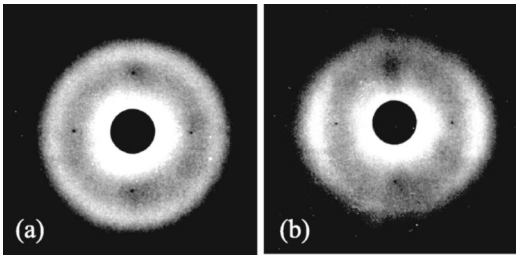

FIG. 5. Two typical x-ray scattering patterns obtained before deformation: (a) $\lambda_{xx}=1$, and at a relatively high imposed strain: (b) $\lambda_{xx}=1.4$ (40% extension). In the first case there is no azimuthal bias from the perfect helical texture viewed along its axis, while the stretched material shows a high degree of average alignment along the stress axis.

director is uniformly distributed along z [the angle $\phi(z)=q_0 z$, cf. Fig. 1]. As the sample is stretched, azimuthal lobes develop, see Fig. 5(b), indicating that there is now a preferred orientation of the nematic director, along the direction of elongation. There is no detectable threshold for lobes to develop, as can be seen from the azimuthal intensity scans shown in Fig. 6(a).

We can, in fact, model these azimuthal intensity profiles by assuming that the cholesteric structure is locally exactly

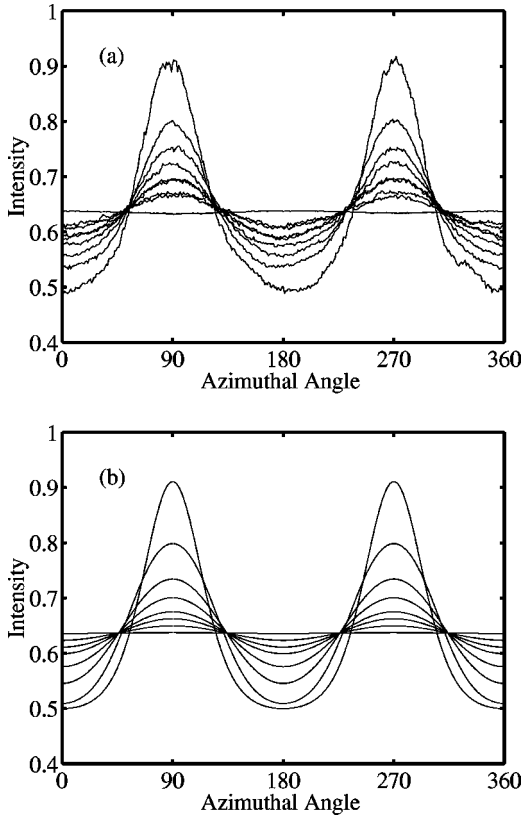

FIG. 6. (a) Azimuthal intensity (arb. units) distribution around the wide-angle diffraction ring for $\lambda_{xx}=1.00, 1.04, 1.08, 1.12, 1.16, 1.24, 1.32$, and 1.40. At $\lambda_{xx}=1.00$, the profile is flat to within our experimental error. The scattering profile showing the highest dependence of intensity on azimuthal angle is obtained from a nematic liquid crystal elastomer. (b) Theoretical prediction from Eq. (3.1) for the same strain values as (a).

the same as that of a chemically similar nematic and then performing the average along the helical pitch. To do so, we need the x-ray scattering data for a corresponding monodomain (aligned) nematic elastomer—which is presented for comparison as the maximal curve in Fig. 6(a); this gives the reasonable value of nematic order parameter $Q\approx 0.5$, calculated by standard methods [19]. One then assumes a stack of such nematic layers along the beam path, continuously rotating by the angle $\phi(z)$. In an ideal cholesteric $\phi=q_0 z$ and the predicted azimuthal distribution is uniform: all director orientations in the plane are equally represented in the scattering.

As soon as an external strain $\lambda=\lambda_{xx}$ is applied, the cholesteric texture is modified, with its angle expressed by the formula derived in Ref. [12],

$$\tan 2\phi=\frac{2\lambda^{1/4}(r-1)\sin 2\tilde{q}z}{(r-1)(\lambda^2+\lambda^{-3/2})\cos 2\tilde{q}z+(r+1)(\lambda^2-\lambda^{-3/2})}. \tag{3.1}$$

This expression is written in a slightly different format than in Ref. [12], using a shorthand λ for the imposed extension λ_{xx} and substituting the calculated value for the transverse sample contraction due to incompressibility, $\lambda_{zz}=\lambda^{-1/4}$. Also, the corresponding affine contraction of the cholesteric pitch is taken into account by taking the wave number $\tilde{q}=\lambda^{1/4}q_0$. Equation (3.1) expresses the strain-induced bias of director orientations along the x direction: the coarsening of the helix occurs (interrupted by the critical jump at λ_c that is the point of zero denominator of $\tan 2\phi$). Taking the value of r as estimated from the stress-strain data in Fig. 4 and the values of imposed strain λ as labeled in Fig. 6(a), we can analytically predict how the azimuthal intensity distribution would evolve, see Fig. 6(b). The agreement is very satisfactory, suggesting that the theoretical description of helix coarsening in CLCE is reasonable.

C. Effects of strain on the photonic structure

It is evident from a comparison of the unstretched sample spectra in Fig. 3 how the sample transmits very differently light of opposite polarizations. In the region of wavelengths around $\Lambda=400$ nm a difference in transmission greater than 2OD (optical density) is measured [20].

Figures 7(a) and 7(b) show the evolution of absorption spectra of right-and left-hand circularly polarized light, respectively, as the sample is uniaxially strained. The data in Fig. 7(a) clearly shows that with no applied strain R^* polarized light is reflected at wavelengths below ~ 500 nm. This gap wavelength shifts downwards as the sample is stretched, as shown in Fig. 8. The transmitted intensity spectra of L^* polarized light in Fig. 7(b) reveal a dramatic development of a new reflection gap centered around ~ 430 nm as soon as the sample is stretched. With further increasing uniaxial strain, at $\lambda>1.04$ the L^* reflection gap appears to have fine structure, the transmitted intensity shows two separate minima, respectively at ~ 390 nm and ~ 440 nm. We remark that as no R^* polarized light is transmitted here, this complementary nearly total reflection of L^* polarized light

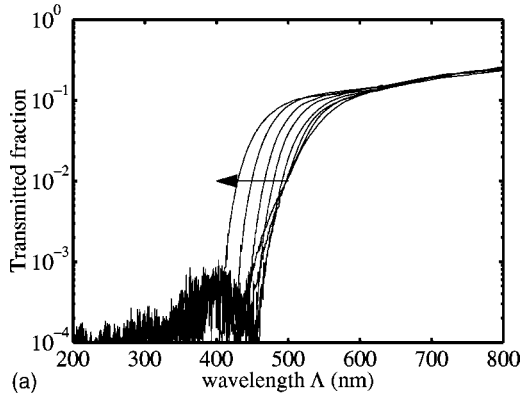

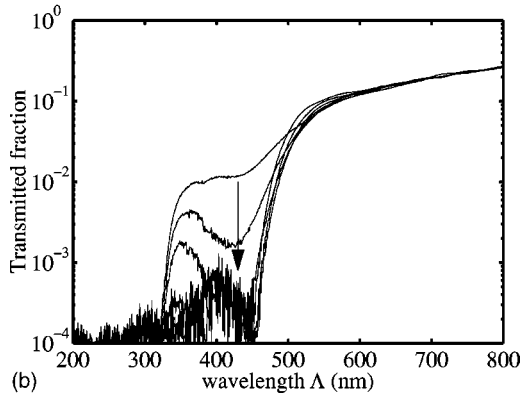

FIG. 7. (a) Helicity R^*. On stretching, the main R^* reflection remains but the line edge sharpens and moves to shorter wavelengths. The spectra are presented at consecutive strains $\lambda_{xx}=1,1.02,1.04,1.08,1.16,1.24,1.40,1.64$, the arrow indicating increasing strain. (b) Helicity L^*. A dip in the transmitted intensity (the new gap) develops under strain, until the sample becomes opaque at that wavelength. The spectra are presented at consecutive strains $\lambda_{xx}=1,1.02,1.04,1.08,1.12,1.16$, the arrow indicating increasing strain.

means that for $\lambda_{xx}>1.04$ the material is not transmitting any light at the wavelengths corresponding to the L* reflection peak. We have measured spectra of transmitted nonpolarized light that confirm this. Above a strain $\lambda=1.08$ the transmitted light spectra of L^* and R^* polarized light are indistinguishable.

D. Effects of strain on the geometry

In an incompressible elastomer, a strain λ_{xx} induces a contraction in *y* and *z* directions. For an isotropic rubber one would expect $\lambda_{yy}=\lambda_{zz}=1/\sqrt{\lambda}$. The pitch of the cholesteric helix, which is probed by absorption of R^* light, is affinely deformed by the contraction in *z*, and the shift of the reflection gap edge is a direct measure of this *z* contraction. We measured the strain-induced shift of the wavelength at which transmission of R^* polarized light is inhibited, Fig. 7(a), and present this data as a function of the strain λ_{xx} in Fig. 8. It is clear that the data are incompatible with the deformation of an isotropic rubber. Instead, the data agrees qualitatively with the prediction from the theory of cholesteric rubber deformation of Ref. [12] and furthermore we are able to confirm the validity of the refined approximation reported by

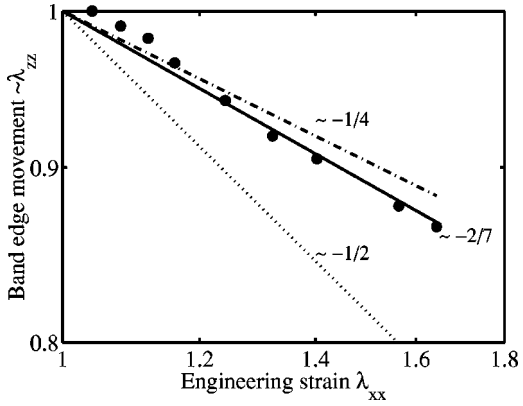

FIG. 8. Shift of the reflection gap edge for R^* polarized light, as a function of applied strain $\lambda=\lambda_{xx}$. This is a measure of the induced contraction λ_{zz}. The dotted line is the contraction for an isotropic rubber $\lambda^{-1/2}$, the dashed line is the theoretical prediction of Ref. [12] $\lambda^{-1/4}$, the solid line is the refined approximation presented in Ref. [15] $\lambda^{-2/7}$.

Ref. [15], which matches the scaling of our data to within experimental error. The underlying asymmetry of mechanical properties, introduced by the cholesteric helix texture, leads to an imbalance between *y* and *z* directions, so effectively the rubber strip is much stiffer along the pitch axis and the stretched cholesteric rubber strip contracts much more in the plane of the director and much less along its thickness: $\lambda_{yy}=\lambda^{-3/4}$ and $\lambda_{zz}=\lambda^{-1/4}$. A refinement [15] of this theoretical prediction, $\lambda_{yy}\approx\lambda^{-2/7}\equiv\lambda^{-0.28}$ fits the experimental data in Fig. 8 even better.

IV. CONCLUSIONS

Qualitative agreement is obvious between the experimental and the theoretical azimuthal intensity profiles, indicating that the predicted helix coarsening is very likely to be a reasonable description of the structure of stretched CLCE systems. Equation (3.1) has been successfully used to evaluate the patterns of x-ray scattering at different degrees of imposed extension and the associated mechanical change λ_{zz} reflected in the gap edge movement.

On increasing strain the cholesteric texture evolves in a predictable way, coarsening into a sequence of nearly uniform director regions, separated by increasingly sharp twist walls. Deviation from the perfectly sinusoidal modulation of optical indicatrice in an undistorted cholesteric can be described as a mixture of higher harmonics and, accordingly, new band gaps emerge in both the ''correct'' (R^* in our case) and the ''opposite'' (L^*) circular polarizations of incident light. The detailed calculation in Ref. [15] gives the particular predictions of photonic structure and its evolution. Our spectral measurements, Figs. 7(a) and 7(b), can be directly compared to the band gaps that occur at the first Brillouin zone boundary. The general behavior, that is predicted in Ref. [15] for smaller wave vectors, would lie in the UV range for our particular material, although the fine structure in the L^* helicity spectra may be a signal of that complexity.

Considering first the circular polarization R^*, the same helicity as the cholesteric itself, our main result is the experi-

mental measure of the scaling of the pitch wavelength as a function of strain Fig. 8: the observed movement of the band edge is $\Lambda_{gap} \sim \lambda^{-2/7}$. In addition, an important observation can be made of the band edge becoming much steeper on deformation. One could imagine that a number of intrinsic imperfections, in particular, the possible wandering of the helical axis away from the sample plane normal, would be reduced by mechanical strain: the cholesteric texture coarsens, but also becomes more perfect, defect-free. This might have importance in lasing and other photonic applications where the increasing of optical purity of the system is of importance. In the case of opposite circular polarization, L^*, we confirm the absence of a band gap for the unstrained material. On deformation we observe the gradual development of such a gap with no apparent threshold.

Several more detailed issues remain outstanding. In particular, this relates to the fine structure of transmission spectra for both R^* and L^* polarizations (we assume it is due to the selective reflection, rather than absorption). The fine structure below 450 nm is evident, as well as the apparent double-peak modulation, both seemingly reproducible between different samples and different stretching events. This modulation, as is the fine structure on top of it, are not necessarily the noise: one can clearly resolve the spectra down to 10^{-4} level in the unstrained sample. Intriguing possible explanations include the effects of randomly quenched disorder (an inherent feature of liquid crystalline elastomers), further modified by deformation and affecting the average light propagation through the cholesteric texture.

To summarize—we have described the combined measurements of optical, structural, and mechanical properties of a cholesteric liquid crystal elastomer and compared with the theoretical predictions of the deformation and the resulting optical effects. The behavior of this class of materials under biaxial strain had been shown to be much simpler and has already found application in photonic devices. The present study confirms our understanding of the effects of a mechanical field and demonstrates the surprisingly rich behavior of these materials as a function of uniaxial strain.

ACKNOWLEDGMENTS

We thank P. A. Bermel and M. Warner for a number of useful discussions. The preparation of materials has been possible due to the advice and help of S. T. Kim and H. Finkelmann. This research has been supported by EPSRC.

[1] M. Warner and E.M. Terentjev, Prog. Polym. Sci. **21**, 853 (1996).
[2] D.L. Thomsen III, P. Keller, J. Naciri, R. Pink, H. Jeon, D. Shenoy, and B.R. Ratna, Macromolecules **34**, 5868 (2001).
[3] H. Finkelmann, E. Nishikawa, G.G. Pereira, and M. Warner, Phys. Rev. Lett. **87**, 015501 (2001).
[4] P. Gennes and J. Prost, *Physics of Liquid Crystals* (Clarendon, Oxford, 1993).
[5] H. Finkelmann and G. Rehage, Abstr. Pap. - Am. Chem. Soc. **186**, 184 (1983).
[6] N.A. Plate, Y.S. Freidzon, and V.P. Shibaev, Pure Appl. Chem. **57**, 1715 (1985).
[7] R. Zentel, G. Reckert, S. Bualek, and H. Kapitza, Macromol. Chem. Phys. **190**, 2869 (1989).
[8] W. Meier and H. Finkelmann, Macromolecules **26**, 1811 (1993).
[9] C.D. Hasson, F.J. Davis, and G.R. Mitchell, Mol. Cryst. Liq. Cryst. Sci. Technol., Sect. A **332**, 2665 (1999).
[10] C.-C. Chang, L.-C. Chien, and R.B. Meyer, Phys. Rev. E **55**, 534 (1997).
[11] S.T. Kim and H. Finkelmann, Macromol. Rapid Commun. **22**, 429 (2001).
[12] M. Warner, E.M. Terentjev, R.B. Meyer, and Y. Mao, Phys. Rev. Lett. **85**, 2320 (2000).
[13] H. Finkelmann, S.T. Kim, A. Munoz, P. Palffy-Muhoray, and B. Taheri, Adv. Mater. **13**, 1069 (2001).
[14] Y. Mao, E.M. Terentjev, and M. Warner, Phys. Rev. E **64**, 041803 (2001).
[15] P.A. Bermel and M. Warner, Phys. Rev. E **65**, 010702 (2002).
[16] E. Hecht, *Optics*, 2nd ed. (Addison-Wesley, Reading, MA, 1987).
[17] H. Finkelmann, A. Greve, and M. Warner, Eur. Phys. J. E **5**, 281 (2001).
[18] S.M. Clarke, A. Hotta, A.R. Tajbakhsh, and E.M. Terentjev, Phys. Rev. E **65**, 021804 (2002).
[19] M. Deutsch, Phys. Rev. A **44**, 8264 (1991).
[20] The optical density (OD) is a unit measuring the effective attenuation of transmitted light, on logarithmic scale, so that a difference of 2OD between R^* and L^* transmitted light intensity means a ratio of 100.